[19] T. Kawamura, J. Suzuki, Y. V. Wang, S. Menendez, L. B. Morera, A. Raya, G. M. Wahl, J. C. Belmonte, *Nature* **2009**, *460*, 1140 – 1144.
[20] M. A. Esteban, T. Wang, B. Qin, J. Yang, D. Qin, J. Cai, W. Li, Z. Weng, J. Chen, S. Ni, K. Chen, Y. Li, X. Liu, J. Xu, S. Zhang, F. Li, W. He, K. Labuda, Y. Song, A. Peterbauer, S. Wolbank, H. Redl, M. Zhong, D. Cai, L. Zeng, D. Pei, *Cell Stem Cell* **2010**, *6*, 71 – 79.
[21] Y. H. Loh, Q. Wu, J. L. Chew, V. B. Vega, W. Zhang, X. Chen, G. Bourque, J. George, B. Leong, J. Liu, K. Y. Wong, K. W. Sung, C. W. Lee, X. D. Zhao, K. P. Chiu, L. Lipovich, V. A. Kuznetsov, P. Robson, L. W. Stanton, C. L. Wei, Y. Ruan, B. Lim, H. H. Ng, *Nat. Genet.* **2006**, *38*, 431 – 440.
[22] S. Yamanaka, *Cell* **2009**, *137*, 13 – 17.
[23] P. H. Huang, C. H. Chen, C. C. Chou, A. M. Sargeant, S. K. Kulp, C. M. Teng, J. C. Byrd, C. S. Chen, *Mol. Pharmacol.* **2011**, *79*, 197 – 206.
[24] M. Minoshima, T. Bando, S. Sasaki, J. Fujimoto, H. Sugiyama, *Nucleic Acids Res.* **2008**, *36*, 2889 – 2894.
[25] C. S. Jacobs, P. B. Dervan, *J. Med. Chem.* **2009**, *52*, 7380 – 7388.
[26] C. C. Wang, U. Ellervik, P. B. Dervan, *Bioorg. Med. Chem.* **2001**, *9*, 653 – 657.
[27] N. R. Wurtz, J. M. Turner, E. E. Baird, P. B. Dervan, *Org. Lett.* **2001**, *3*, 1201 – 1203.
[28] M. Minoshima, T. Bando, S. Sasaki, K. Shinohara, T. Shimizu, J. Fujimoto, H. Sugiyama, *J. Am. Chem. Soc.* **2007**, *129*, 5384 – 5390.

Received: September 22, 2011
Published online on October 28, 2011

特集　癌幹細胞の実態と治療戦略

2．病態
3）癌幹細胞のエピジェネティック制御

山田泰広*

ほぼすべての癌において，DNA (deoxyribonucleic acid) メチル化異常などのエピジェネティック修飾異常が観察される。しかし，発癌過程におけるエピジェネティック制御異常の役割については，未だ不明な点が多い。改変可能なエピジェネティック修飾は癌治療の標的として有望であることから，発癌に関わるエピジェネティック制御異常を同定し，理解することは，癌幹細胞を標的とした新たな治療方法開発にもつながることが期待される。本稿では，近年の研究により，徐々に明らかになりつつある，癌細胞のエピジェネティック制御機構の意義や，筆者らの取り組みについて紹介する。

1．エピジェネティック修飾異常の特徴

ほぼすべての癌において，DNA (deoxyribonucleic acid) 塩基配列の異常とともにDNAメチル化異常などのエピジェネティック修飾異常が観察される[1]。現在までにリバースジェネティクスを用いた手法などにより，DNA塩基配列の異常が発癌の原因であることが示されてきた。一方で，癌細胞におけるエピジェネティック制御異常がどのようにして，またどの程度発癌に関与しているかは，未だ不明な点が多い。改変可能なエピジェネティック修飾は癌治療の標的として有望であり，発癌に関わるエピジェネティック制御異常を同定することは，新たな治療方法開発にもつながる可能性が期待される。

癌細胞におけるエピジェネティック修飾異常において，これまでDNAメチル化異常が最も盛んに研究されてきた。癌細胞におけるDNAメチル化異常は大きく分けて二つの特徴がある。癌細胞では，ゲノムワイドに見るとメチル化DNAの総量は低下しているにも関わらず，特定部位，特に遺伝子のプロモーター領域のCG配列が豊富な領域においては高メチル化状態が観察される。現在までの研究により，ゲノムワイドなDNA低メチル化状態は，ゲノムの不安定性を引き起こすことで，染色体異常を誘発し，発癌を促進することが示唆されている[2][3]。一方で，部位特異的なDNA高メチル化は，癌抑制遺伝子のプロモーター領域に頻繁に観察され，癌抑制遺伝子の転写抑制に関与して発癌促進的に働いていることが示されている。実際に大腸発癌のモデルマウスにおいてDNAメチル化レベルを低下させると，非常に強い発癌抑制作用を示すことが報告されている[4]~[6]。(図1)。DNAメチル化レベル低下による発癌抑制作用は，大腸のみならず，舌，食道，胃の消化管発癌においても確認されており，DNA脱メチル化剤の発癌抑制における有用性が示唆されている[7][8]。特にDNA脱メチル化剤は骨髄異型性症候群(MDS)

*京都大学iPS細胞研究所（CiRA）初期化機構研究部門・特定拠点教授（やまだ・やすひろ）

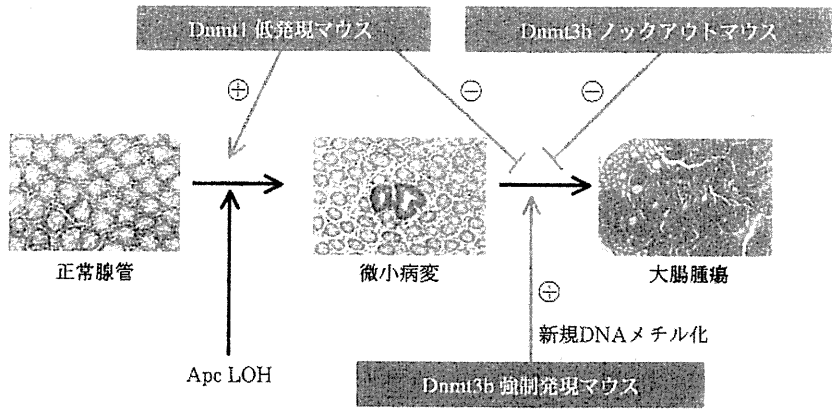

図1　DNA メチル化によるマウス大腸発癌過程への修飾
DNA メチル化の低下は，微小病変から大腸腫瘤への進展を強く抑制する．
DNA：deoxyribonucleic acid，LOH：loss of heterozygosity
Dnmt：DNA メチル基転移酵素

（文献4～6，9より）

の治療に有用であることが示され，既に臨床応用されている。このように，DNA メチル化修飾を標的とした癌治療法の開発が期待されている。

しかしながら，一方で DNA 低メチル化状態は肝臓や線維芽細胞などにおいては発癌を促進することが示されている[2)5)]。これは DNA 低メチル化状態によるゲノムの不安定性に起因することが予想される。すなわち，非特異的な DNA メチル化の抑制は，臓器によっては発癌促進的に作用する可能性が示されている。発癌には Dnmt3b による部位特異的な DNA メチル化の関与が示唆されている[9)]。現在，部位特異的に DNA メチル化を制御する技術開発も行われており，より安全で効率的な癌治療方法開発に結びつく可能性がある。そのためにも，癌細胞における DNA メチル化異常，そしてその意義に関する詳細な理解が必要であろう。

2．DNA メチル化異常の起源

以上のように，DNA メチル化異常が発癌に重要な役割を果たしていることが明らかになりつつあるものの，どのようにしてメチル化異常などのエピジェネティック修飾異常が引き起こされるのかは不明な点が多い。DNA メチル化を含むエピジェネティック修飾は遺伝子の転写状態と密接な関連があり，一部のエピジェネティック修飾変化は，遺伝子転写状態の変化の結果として引き起こされている可能性などが考えられている[10)]。さらに近年，炎症と DNA メチル化異常との関連が注目されている。炎症により DNA メチル化異常が誘発されることが明らかとなり，その DNA メチル化異常は，癌細胞に観察される DNA メチル化異常と類似していることが示された。興味深いことに，一見正常に見える前癌状態の細胞には，既に癌細胞で観察される DNA メチル化異常と類似した異常が観察されることが知られている。すなわち，炎症により誘発される DNA メチル化異常を有する細胞は発癌の母地となっている可能性があり，epigenetic field for cancerization の概念が提唱されている[11)]。

例えば，胃では，ヘリコバクターピロリの感染と胃発癌の関連が示されており，ヘリコバクター感染による炎症が DNA メチル化異常を介して発癌の素地を形成している可能性が考えられる[12)]。他にも大腸発癌など，炎症と密接に関連した発癌が数多くあり，これらの発癌にも，炎症により引き起こされた DNA メチル化異常が発癌促進的に作用していることが予想される[13)]。発癌過程にお

MDS：骨髄異型性症候群，iPS 細胞：人工多能性幹細胞

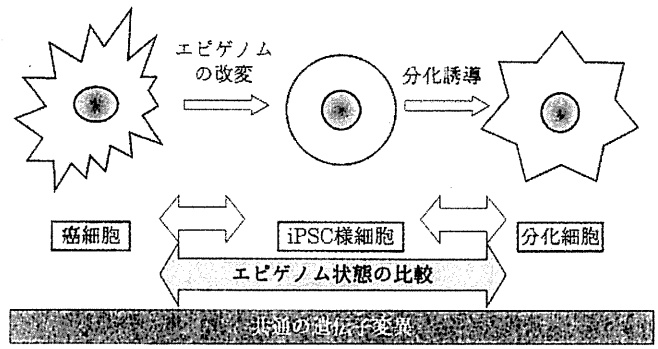

図2 iPS細胞作製技術を用いた癌研究
iPS細胞作製技術により癌細胞のエピジェネティック制御状態を強制的に改変し，その役割解明を目指す．
iPS細胞：人工多能性幹細胞
（筆者作成）

ける周囲環境からのnon-cell autonomousな影響が注目されてきたが，そこにはエピジェネティック修飾状態の変化が関与しているのかもしれない。

3．癌幹細胞のheterogeneityと癌幹細胞

近年，癌細胞のheterogeneityが注目されている。一つの腫瘤の中でも異なる性質を持った癌細胞が存在し，腫瘤形成に対して，より重要な役割を持つ細胞集団が存在することが示唆されており，癌幹細胞の概念として定着しつつある。癌細胞のモノクローナリティを考えれば，同一腫瘤内の遺伝子配列異常は，基本的には共通であると考えられる。従って，腫瘤内の癌細胞のheterogeneityはエピジェネティック制御状態の違いにより引き起こされている可能性が予想される。癌幹細胞の治療抵抗性を示唆する研究結果が数多く報告され，癌幹細胞を標的とした癌治療法開発が望まれている。癌幹細胞におけるエピゲノム制御機構を明らかにすることで，そのエピゲノム修飾を標的として，癌幹細胞の分化状態に変化を誘導し，幹細胞としての自己増殖能を制御できる可能性がある。実際に，筆者らの最近の研究により，DNAメチル化状態の変化が腫瘍細胞の分化状態に影響を与えることが明らかになりつつあり，エピジェネティック制御による分化誘導を介した癌治療が期待される。

4．リプログラミング技術を用いた癌細胞のエピジェネティクス研究

体細胞に4つの転写因子を導入することで，多能性を持つ**iPS細胞**（人工多能性幹細胞）を樹立できるようになった[14]。iPS細胞の樹立過程には，エピジェネティック修飾状態の大きな改変を伴うため，iPS細胞作製技術はエピジェネティック制御状態を積極的に改変させるツールとして利用可能である。従って，iPS細胞作製技術を癌細胞に応用することで，癌細胞のエピジェネティック制御状態を積極的に変化させることが可能であると考えられる。（**図2**）。実際に核移植によるリプログラミング法を用いて，悪性黒色腫の核を初期化した後，再分化させることで，悪性黒色腫の遺伝子配列異常を持った非腫瘍性のメラノサイトを作製できることが示されている[15]。iPS細胞作製技術を含む細胞リプログラミング技術は，癌細胞のエピジェネティック制御機構の意義解明に有用のみならず，癌細胞の治療に応用できる可能性がある。

5．まとめ

以上のように，近年癌細胞のエピジェネティック制御機構の意義解明に関する研究が盛んに行われている。修飾可能なエピジェネティック制御は，新たな癌予防法，および癌治療法に有用であることが示唆されている。効果的な予防法，治療

法開発のために，癌細胞におけるエピジェネティック制御機構の更なる理解が必須であろう。

文　献

1) Jones PA, Baylin SB : The epigenomics of cancer. Cell **128** (4) : 683-692, 2007.
2) Eden A, Gaudet F, Waghmare A, et al : Chromosomal instability and tumors promoted by DNA hypomethylation. Science **300** (5618) : 455, 2003.
3) Gaudet F, et al : Induction of tumors in mice by genomic hypomethylation. Science **300** (5618) : 489-492, 2003.
4) Laird PW, et al : Suppression of intestinal neoplasia by DNA hypomethylation. Cell **81** (2) : 197-205, 1995.
5) Yamada Y, et al : Opposing effects of DNA hypomethylation on intestinal and liver carcinogenesis. Proc Natl Acad Sci U S A **102** (38) : 13580-13585, 2005.
6) Lin H, et al : Suppression of intestinal neoplasia by deletion of Dnmt3b. Mol Cell Biol **26** (8) : 2976-2983, 2006.
7) Baba S, et al : Global DNA hypomethylation suppresses squamous carcinogenesis in the tongue and esophagus. Cancer Sci **100** (7) : 1186-1191, 2009.
8) Tomita H, et al : Suppressive effect of global DNA hypomethylation on gastric carcinogenesis. Carcinogenesis **31** (9) : 1627-1633, 2010.
9) Linhart HG, et al : Dnmt3b promotes tumorigenesis *in vivo* by gene-specific de novo methylation and transcriptional silencing. Genes Dev **21** (23) : 3110-3122, 2007.
10) Takeshima H, Yamashita S, Shimazu T, et al : The presence of RNA polymerase Ⅱ, active or stalled, predicts epigenetic fate of promoter CpG islands. Genome Res **19** (11) : 1974-1982, 2009.
11) Ushijima T : Epigenetic field for cancerization. J Biochem Mol Biol **40** (2) : 142-150, 2007.
12) Hur K, et al : Insufficient role of cell proliferation in aberrant DNA methylation induction and involvement of specific types of inflammation. Carcinogenesis **32** (1) : 35-41, 2011.
13) Katsurano M, et al : Early-stage formation of an epigenetic field defect in a mouse colitis model, and non-essential roles of T- and B-cells in DNA methylation induction. Oncogene advance online publication 20 June 2011;doi: 10.1038/onc.2011.241.
14) Takahashi K, Yamanaka S : Induction of pluripotent stem cells from mouse embryonic and adult fibroblast cultures by defined factors. Cell **126** (4) : 663-676, 2006.
15) Hochedlinger K, et al : Reprogramming of a melanoma genome by nuclear transplantation. Genes Dev **18** (15) : 1875-1885, 2004.

Cancer Science
The official journal of the Japanese Cancer Association JCA

Combination use of anti-CD133 antibody and SSA lectin can effectively enrich cells with high tumorigenicity

Kenta Moriwaki,[1,6] Kumiko Okudo,[1,6] Naotsugu Haraguchi,[2] Shunsaku Takeishi,[3] Hiromichi Sawaki,[4] Hisashi Narimatsu,[4] Masahiro Tanemura,[2] Hideshi Ishii,[2] Masaki Mori[2] and Eiji Miyoshi[1,5]

Departments of [1]Molecular Biochemistry and Clinical Investigation, [2]Gastroenterological Surgery, Osaka University Graduate School of Medicine, Osaka; [3]GP Biosciences Ltd, Kanagawa; [4]Research Center for Medical Glycoscience, National Institute of Advanced Industrial Science and Technology, Ibaraki, Japan

(Received November 15, 2010/Revised February 21, 2011/Accepted February 28, 2011/Accepted manuscript online March 10, 2011/Article first published online April 14, 2011)

Glycans exhibit characteristic changes in their structures during development and thus have been used as markers for stem/progenitor cells. However, the glycan structures unique to cancer stem cells (CSC) remain unknown. In the present study, we examined glycan structures in CD133$^+$CD13$^+$ CSC, which were recently found to have a high CSC ability, by means of a lectin microarray. Seven sialylated glycan-recognizing lectins, MAL-I, SNA, SSA, TJA-I, ACG, ABA and MAH, showed higher affinity to CD133$^+$CD13$^+$ CSC than CD133$^+$ cells with a lower CSC ability. In addition, we demonstrated that CD133$^+$SSA$^+$ cells isolated from Huh7 cells had a significantly higher ability to form tumors in non-obese diabetic/severe combined immunodeficiency disease (NOD/SCID) mice and spheres under serum-free conditions than CD133$^+$SSA$^-$ cells. These results suggest that hepatic CSC highly express sialylated glycans and that SSA lectin can be used as a tool for isolating CSC. This study is the first report to demonstrate the characteristic glycan structures in CSC and to indicate a new methodology involving lectins for isolating CSC. (*Cancer Sci* 2011; 102: 1164–1170)

A growing body of evidence has suggested that tumors are frequently composed of heterogeneous cell types, and that tumor initiation and growth are driven by a small subset of cells, termed cancer stem cells (CSC) or tumor-initiating cells.[1,2] Cancer stem cells can self-renew and also give rise to more differentiated progeny that comprise the bulk of a tumor.[3] Furthermore, several lines of research have indicated that CSC can be preferentially resistant to many current therapies, including various chemotherapeutic agents and radiation treatment.[4,5] Thus, therapeutic strategies that effectively target CSC could have a major impact on the survival of cancer patients. Evidence of tumor heterogeneity and CSC was first obtained from acute myeloid leukemia[6] and more recently extended to several human solid tumors, for example, breast,[7] brain,[8,9] prostate,[10] colon[11–13] and pancreatic[14] cancers. Over the last decade, a large body of literature has implicated CD133 as a bona fide marker for CSC in some cancers.[8,11,12] However, the validity of CD133 has been a matter of debate since recent studies showed the limitation of isolating CSC using only CD133 as a CSC marker.[15] We reported that the CD133$^+$CD44$^+$ population in colon cancer exhibited higher tumorigenicity than the CD133$^+$CD44$^-$ one,[16] suggesting that it would be much better to use CD133 in combination with other markers to identify CSC. Under these circumstances, we recently found that CD13 was a novel marker for hepatic CSC. The CD133$^+$CD13$^+$ population in hepatoma cell lines and hepatocellular carcinoma (HCC) tissues exhibits higher tumorigenic and self-renewal properties than the CD133$^+$CD13$^-$ one, indicating that HCC-initiating cells are highly enriched in the CD133$^+$CD13$^+$ population.[17]

Glycans often become attached to proteins and lipids on the cell surface, and then structurally and functionally modify these molecules. Glycans consist of several kinds of monosaccharides and show great structural diversity. Research in the field of glycobiology has revealed diverse and complex biological roles for these glycans.[18] The structures and amounts of glycan present on the cell surface dramatically change during development and differentiation.[19] Some of the glycan structures are specific to undifferentiated embryonic stem (ES) cells and thus can be used as markers for these cells. Stage-specific embryonic antigen-1 (SSEA-1) is known to be a marker for mouse ES cells.[20] In addition, human ES cells express SSEA-3, SSEA-4, TRA-1-60 antigen and TRA-1-81 antigen, which can be used as markers for human ES cells.[21] However, the typical glycan structures in CSC remain to be elucidated.

Sialic acids comprise one of the building blocks of glycans, and are generally found at the outermost ends of the glycan chains of glycoproteins and glycolipids. Thus, sialic acids are associated with many physiological and pathological events, including binding with infectious pathogens, regulation of immune responses and tumor malignancy.[22] In particular, alteration of sialic acids is associated with cancer cell behavior, such as invasiveness and metastasis.[23–25]

In the present study, we investigated the characteristic glycan structures in CD133$^+$CD13$^+$ CSC, which have a high tumor-initiating property, isolated from a human hepatoma cell line, Huh7 cells. In addition, the availability of glycans on the cell surface as possible markers for CSC was examined.

Materials and Methods

Cell culture. Human liver cancer cell line Huh7 was purchased from American Type Culture Collection (ATCC, Manassas, VA, USA) and cultured in RPMI 1640 (Sigma, St. Louis, MO, USA) medium containing 10% FCS (Invitrogen, Carlsbad, CA, USA), supplemented with 100 units/mL penicillin G and 100 mg/mL streptomycin, followed by incubation at 37°C under a humidified atmosphere containing 5% CO_2.

Flow cytometric analysis and fluorescence-activated cell sorting (FACS). For surface marker analysis with a flow cytometer, confluent cells in 10-cm dishes were washed once with phosphate-buffered saline (PBS) and then dissociated using PBS containing 1 mM EDTA. After centrifugation, 1×10^6 cells were suspended in 100 μL PBS containing 0.1% BSA, followed

[5]To whom correspondence should be addressed.
E-mail: emiyoshi@sahs.med.osaka-u.ac.jp
[6]These authors contributed equally to this work.

doi: 10.1111/j.1349-7006.2011.01923.x

Table 1. The tumor-initiating ability of $CD133^+CD13^-SSA^-$ and $CD133^+CD13^-SSA^+$ cells among Huh7 cells

	1×10^2 cells	5×10^2 cells	1×10^3 cells	5×10^3 cells
$CD133^+CD13^-SSA^-$	1/8	1/8	2/8	2/8
$CD133^+CD13^-SSA^+$	4/8	6/8	8/8	8/8

by incubation for 40 min at 4°C with the following antibodies: allophycocyanin (APC)-conjugated anti-human CD133 (eBioscience, San Diego, CA, USA), phycoerythrin (PE)-conjugated anti-human CD13 (BD Biosciences, San Jose, CA, USA), and FITC-conjugated SSA lectin (Seikagaku Corp., Tokyo, Japan), which recognizes α2,6-sialylated glycans. Isotype-matched mouse IgG was used as a control (BD Biosciences). Doublet cells were eliminated using FSC-A/FSC-H and SSC-A/SSC-H. Dead cells were eliminated with 7-amino-actinomycin D (BD Biosciences). For FACS cell sorting, $5–10 \times 10^6$ cells were stained as described above and then sorted using FACS BD Aria II (BD Biosciences).

Lectin microarray. The total patterns of oligosaccharide structures in $CD133^+CD13^-$ and $CD133^+CD13^+$ cells were investigated by means of evanescent-field fluorescence-assisted lectin microarray. Forty-five kinds of lectin were immobilized on a glass slide in triplicate. The procedure was described in detail in a previous report.[26] Briefly, cellular proteins in PBS containing 1% Triton X-100 were labeled with Cy3-succimidyl ester (GE Healthcare, Chalfont St. Giles, UK) at room temperature for 1 h in the dark. Excess reagent was removed by gel filtration chromatography. The resultant Cy3-labeled protein solution (100 μL, 250 ng/mL or 2 μg/mL) was applied to a lectin microarray. After incubation at 20°C for 15 h, the glass slide was scanned with an evanescent-field fluorescence scanner, GlycoStation (GP Biosciences Ltd, Kanagawa, Japan). All of the data were analyzed with ARRAY PRO ANALYZER version 4.5 (Media Cybernetics, Inc., Bethesda, MD, USA). The net intensity value for each spot was calculated by subtracting the background value. The signal intensity value for each lectin was expressed as the average of the net intensity values for three spots. The WGA signals were used to normalize the signal intensity of each lectin, because binding to WGA lectin was relatively stable and almost the same in many kinds of cells.

Multiple quantitative PCR array for glycogenes. Multiple quantitative PCR array was performed as previously described.[27,28] Briefly, total RNA was extracted from $CD133^+CD13^-$ and $CD133^+CD13^+$ cells. cDNA was synthesized from 1 μg of total RNA and then subjected to a multiple quantitative PCR array carrying 186 glycogenes and three housekeeping genes. Absolute copy numbers of transcripts in 7.5 ng of total RNA were plotted on a log scale. Genes with a number of transcripts smaller than 100 were omitted from our results due to quite low expression.

***In vivo* tumorigenicity analysis.** Various numbers of cells, ranging from 100 to 5000, were prepared and suspended in 200 μL of RPMI1640 medium and Matrigel (BD Biosciences) mixture (1:1 volume) for injection. These cells were subcutaneously injected into the abdominal and dorsal regions of 6-week-old female non-obese diabetic/severe combined immunodeficiency disease (NOD/SCID) mice (Charles River, Wilmington, MA, USA). Tumor formation was monitored weekly for up to 30 days. An independent special pathologist confirmed tumor formation by examining the histology of HE-stained tissues. The data from two independent experiments are summarized in Table 1.

Sphere formation assay. Cells were seeded on non-coated 6-cm culture dishes (AGC Techno Glass, Chiba, Japan) at 4×10^4 cells per dish in serum-free DMEM/F-12 medium (Invitrogen) containing 20 ng/mL epithelial growth factor (Sigma-Aldrich, St. Louis, MO, USA), 10 ng/mL fibroblast growth factor-2 (Collaborative Biomedical Products, Bedford, MA, USA), 0.4% BSA, B27 NeuroMix (PAA Laboratories, Pasching, Austria), 100 units/mL penicillin G and 100 mg/mL streptomycin. B27 NeuroMix contains vitamins, hormones and other growth factors including insulin, transferrin, catalase, antioxidants and fatty acids. The culture medium was changed every 3 days. After 10 days, each dish was examined under a light microscope and spheroid colonies were measured. The ratio of the area of each spheroid colony to the visual field was calculated. Data are represented as the means of two independent experiments and relative values on the basis of the proportion of $CD133^+CD13^-SSA^-$ cells.

Results

Glycan profiling of $CD133^+CD13^+$ CSC from Huh7 cells using a lectin microarray. We recently reported that $CD133^+CD13^+$ cells exhibit the characteristics of CSC including self-renewal and high tumorigenic abilities.[17] To determine glycan structures unique to hepatic CSC, $CD133^+CD13^+$ cells isolated from Huh7 cells were used as model cells of CSC. $CD133^+CD13^+$ and $CD133^+$ $CD13^-$ cells were isolated from Huh7 cells using FACS, and then 25 ng of Cy3-labeled proteins derived from these cells was subjected to lectin microarray analysis (Fig. 1A). Interestingly, the intensities of five sialylated glycan-recognizing lectins (SNA, SSA, TJA-1, ACG and ABA) among 45 lectins were significantly higher in $CD133^+CD13^+$ cells than $CD133^+CD13^-$ ones. The intensities of several lectins were under the detection limit in the used assay conditions. Thus, next we performed the same experiment using 200 ng of the Cy3-labeled proteins. As shown in Figure 1B, MAL-I and MAH, which recognize sialylated glycans, exhibited higher affinity to $CD133^+CD13^+$ cells than $CD133^+CD13^-$ ones. The intensities of seven sialylated glycan-recognizing lectins are summarized in Figure 2. The results indicate that sialylated glycans are structures unique to $CD133^+CD13^+$ CSC.

Expression profile of glycogenes in $CD133^+CD13^-$ and $CD133^+CD13^+$ cells isolated from Huh7. Next, we searched for genes responsible for the enhanced expression of sialylated glycans in $CD133^+CD13^+$ CSC. The human genome contains approximately several hundred glycogenes. We previously established multiplex quantitative PCR (qPCR) array format for comprehensive profiling of an expression pattern of glycogenes. The qPCR array consists of probes and primer sets for measuring mRNA of 186 glycogenes, and enables the determination of expression profiles for these glycogenes in a single assay. An expression profile of 186 glycogenes were analyzed and compared between $CD133^+CD13^-$ and $CD133^+CD13^+$ cells (Table S1). As shown in Figure 3, eight genes were differentially expressed more than twofold between both cells. Seven genes, HS6ST1, ST6GALNAC1, B4GALT5, GALNT13, GCNT3, GCNT4 and B4GALNT2, were expressed at an elevated level in $CD133^+CD13^+$ cells. In contrast, only DPAGT1 is highly expressed in $CD133^+CD13^-$ cells. Among the eight genes, ST6GALNAC1 exhibited the biggest difference (4.385-fold higher in $CD133^+CD13^+$ cells) and was the only glycogene involved in sialylation. Thus, this result suggests that ST6GALNAC1 is a gene responsible for high expression of sialylated glycans in $CD133^+CD13^+$ cells.

$CD133^+CD13^+$ CSC were present in the SSA-positive population. To confirm the sialylation level in $CD133^+CD13^+$ CSC, we performed flow cytometric analysis using anti-CD133 and CD13 antibodies, and several sialylated glycan-recognizing lectin. As previously reported, $CD133^+CD13^+$ CSC comprised a very minor population of Huh7 cells (Fig. 4A). These cells were invariably present in the SSA-positive population

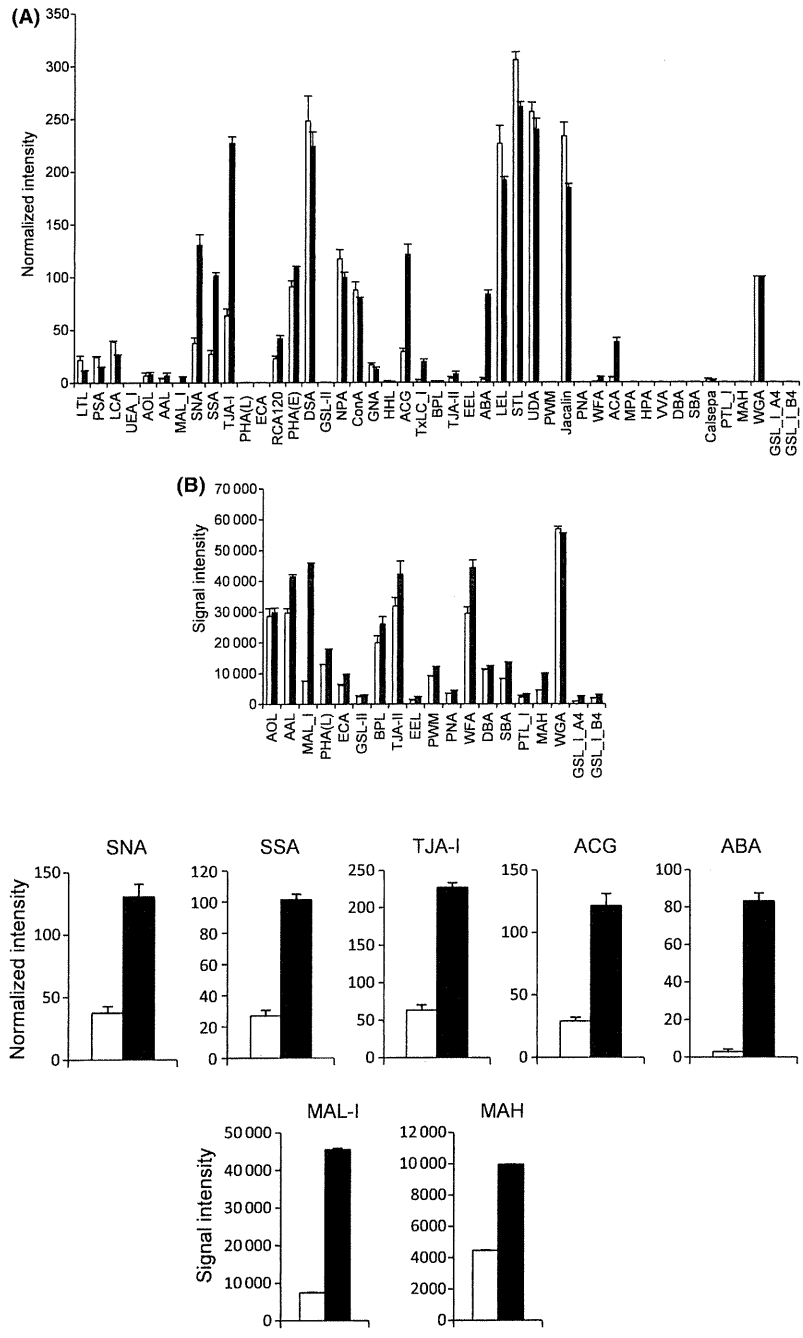

Fig. 1. Differential glycan profiling of $CD133^+CD13^-$ and $CD133^+CD13^+$ cells using a lectin microarray. (A) Aliquots of 25 ng of Cy3-labeled proteins were applied to a lectin microarray. The fluorescence intensity of each lectin was normalized to the intensity of WGA. (B) Aliquots of 200 ng of Cy3-labeled proteins were applied to a lectin microarray. The fluorescence intensity of each lectin was directly indicated because of the saturation of the fluorescence intensity of WGA. The fluorescence intensities of lectins with $CD133^+CD13^-$ and $CD133^+CD13^+$ cells are indicated by white and black columns, respectively. Bars, SD.

Fig. 2. Focused differential glycan profiling of $CD133^+CD13^-$ and $CD133^+CD13^+$ cells. The fluorescence intensities of sialylated glycan-recognizing lectins among 45 lectins were focused. The fluorescence intensities of lectins with $CD133^+CD13^-$ and $CD133^+CD13^+$ cells are indicated by white and black columns, respectively. Bars, SD.

(Fig. 4B). Other lectins showed almost equal binding to both $CD133^+CD13^-$ and $CD133^+CD13^+$ cells (data not shown). The SSA lectin recognizes α2,6-sialylated glycans. These results confirmed that $CD133^+CD13^+$ CSC highly express α2,6-sialylated glycans recognized by SSA lectin on their surface.

$CD133^+CD13^-SSA^+$ cells efficiently generated tumors in NOD/SCID mice. Next, we investigated whether SSA lectin can be used for the isolation of hepatic CSC. As shown in Figure 4B, the $CD133^+SSA^+$ population, but not the $CD133^+SSA^-$ one, definitely includes $CD133^+CD13^+$ CSC. Because $CD133^+CD13^+$ CSC have already been revealed to exhibit strong CSC ability,[17] the $CD133^+CD13^-$ population was divided into SSA-positive and negative cells to eliminate an effect of $CD133^+CD13^+$ CSC. $CD133^+CD13^-SSA^+$ and $CD133^+CD13^-SSA^-$ cells were isolated from Huh7 cells (Fig. 5A), and then various numbers of isolated cells, ranging from 100 to 5000, were subcutaneously inoculated into NOD/SCID mice. A significant difference in tumorigenicity was observed between these two subpopulations (Fig. 5B). Tumor formation was observed in four of eight mice on injection of as few as 1×10^2 $CD133^+CD13^-SSA^+$ cells. In contrast, only one mouse injected with 1×10^2 $CD133^+CD13^-SSA^-$ cells showed generation of a tumor. In addition, the injection of $CD133^+CD13^-SSA^+$ cells at a higher dose (dose range: 5×10^2–5×10^3) generated a much larger tumor than that of the $CD133^+CD13^-SSA^-$ ones. The data are summarized in Table 1. These results indicate that $CD133^+CD13^-SSA^+$ cells have a significantly higher tumor-initiating property than the $CD133^+CD13^-SSA^-$ ones.

doi: 10.1111/j.1349-7006.2011.01923.x

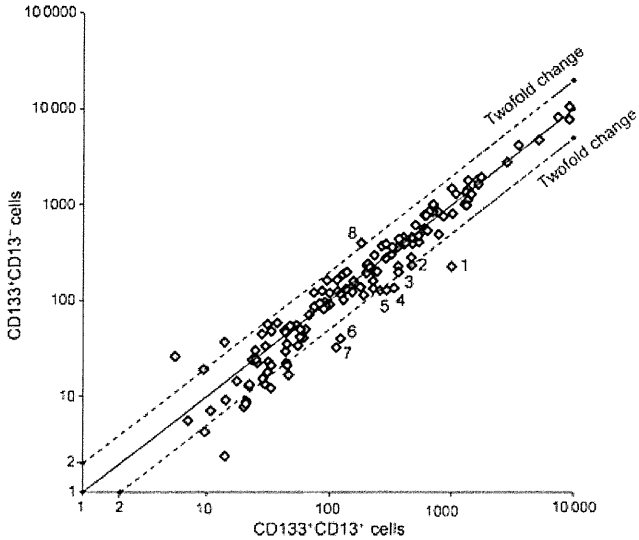

Fig. 3. Differential expression profiling of 186 glycogenes between $CD133^+CD13^-$ and $CD133^+CD13^+$ cells. Absolute copy number of transcripts in 7.5 ng of total RNA derived from $CD133^+CD13^-$ and $CD133^+CD13^+$ cells was determined by qPCR array analysis and scatter-plotted using a log scale. Differentially expressed genes more than twofold are numbered. 1, ST6GALNAC1; 2, B4GALT5; 3, GCNT4; 4, GCNT3; 5, GALNT13; 6, HS6ST1; 7, B4GALNT2; 8, DPAGT1. Genes with a number of transcripts smaller than 100 were omitted from our results due to quite low expression.

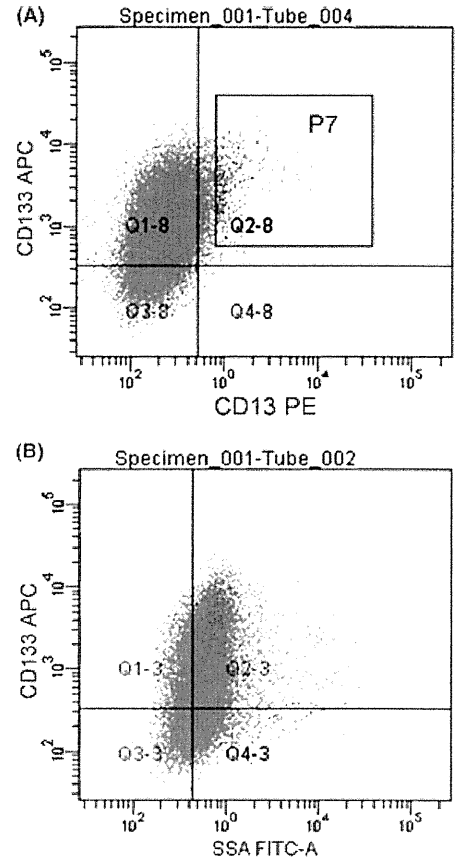

Fig. 4. Expression of CD133, CD13 and α2,6-sialylated glycans on the surface of Huh7 cells. Cells were stained with allophycocyanin (APC)-conjugated anti-CD133 antibody, phycoerythrin (PE)-conjugated anti-CD13 antibody and FITC-conjugated SSA lectin, and then analyzed by FACS. The horizontal and vertical axes denote the expression level of each molecule. (A) $CD133^+CD13^+$ cells, which exhibit a high potential as CSC, are gated in P7 and indicated in blue. (B) $CD133^+CD13^+$ cells were limited to the SSA-positive fraction.

$CD133^+CD13^-SSA^+$ cells efficiently formed sphere *in vitro*. Because numerous previous studies demonstrated that the formation of spheres in serum-free medium is one of the characteristics of CSC, $CD133^+CD13^-SSA^+$ and $CD133^+CD13^-SSA^-$ cells were cultured under stem cell-selective conditions. $CD133^+CD13^-SSA^+$ cells had aggregated into floating spheroid clusters after 10 days when the cells were cultured on non-coated dishes in serum-free Ham F12 supplemented with EGF, FGF-2 and B27 NeuroMix (Fig. 6A). In contrast, we observed little formation of spheres by $CD133^+CD13^-SSA^-$ cells cultured under the same conditions. The quantitative analysis showed a significant increase of sphere formation in $CD133^+CD13^-SSA^+$ cells compared with the $CD133^+CD13^-SSA^-$ ones (Fig. 6B). This finding demonstrates that $CD133^+CD13^-SSA^+$ cells have a higher CSC property than the $CD133^+CD13^-SSA^-$ ones.

Discussion

In order to identify the characteristic glycan structures in CSC, we used the lectin microarray system, which is an emerging technique for the profiling of entire cellular glycan structures. Due to its extremely high sensitivity, this method is the best tool for analyzing glycan structures in a small number of cells, like CSC. In the present study, a lectin microarray showed that all of seven sialic acid-recognizing lectins, MAL-I, SNA, SSA, TJA-1, ACG, ABA and MAH, more strongly bound to $CD133^+CD13^+$ CSC from Huh7 cells than $CD133^+CD13^-$ cells. A similar result was obtained in another hepatoma cell line, Hep3B (Figs S1,S2). MAL-I and MAH recognize α2,3-sialic acid residues. ACG exhibits a higher affinity to α2,3-sialylated and high branched *N*-glycans than non-sialylated ones. ABA exhibits an affinity to sialylated T-antigen (Neu-Acα2,3Galβ1,3GalNAc). In contrast, SNA, SSA and TJA-1 recognize α2,6-sialic acid residues. These findings strongly suggest that sialylated glycans are the characteristic structures of CSC. In future studies, it would be required to reveal the structures of the sialylated glycans expressed on $CD133^+CD13^+$ CSC in detail. Moreover, in the present study, it was revealed that SSA lectin could be used as an additional marker for isolating CSC. Future studies should also examine whether other lectins, such as α2,3-sialic acid-recognizing ones, could be possible markers for isolating CSC.

When a difference of more than twofold was defined to be significant, the lectin microarray also exhibited a high affinity of TxLC-I, ACA, GSL-I-A4 to $CD133^+CD13^+$ CSC. TxLC-I recognizes a relatively broad range of structures, including galactosylated and agalactosylated *N*-glycan. ACA also recognizes agalactosyl *N*-glycan. Interestingly, TxLC-I and ACA can also bind to sialylated glycans, especially α2,6 sialic acid and sTn antigen, respectively. Thus, a high affinity of both lectins might be caused by the increased expression of sialylated glycans in $CD133^+CD13^+$ CSC. GSL-I-A4 recognizes α-linked GalNAc on *O*-glycan. While the meaning of high affinity of GSL-I-A4 to $CD133^+CD13^+$ CSC remains unclear, the change of sialylated glycans was the most common and drastic in $CD133^+CD13^+$ CSC.

Glycosylation is regulated by the complicated mechanisms involving many kinds of glycogenes, such as glycosyltranefe-rases, sugar nucleotide-synthetic enzymes, and sugar nucleotide transporters. Thus, comprehensive analysis is required for a detailed understanding of the regulatory mechanisms of glycosylation. A DNA microarray has been used as a comprehensive

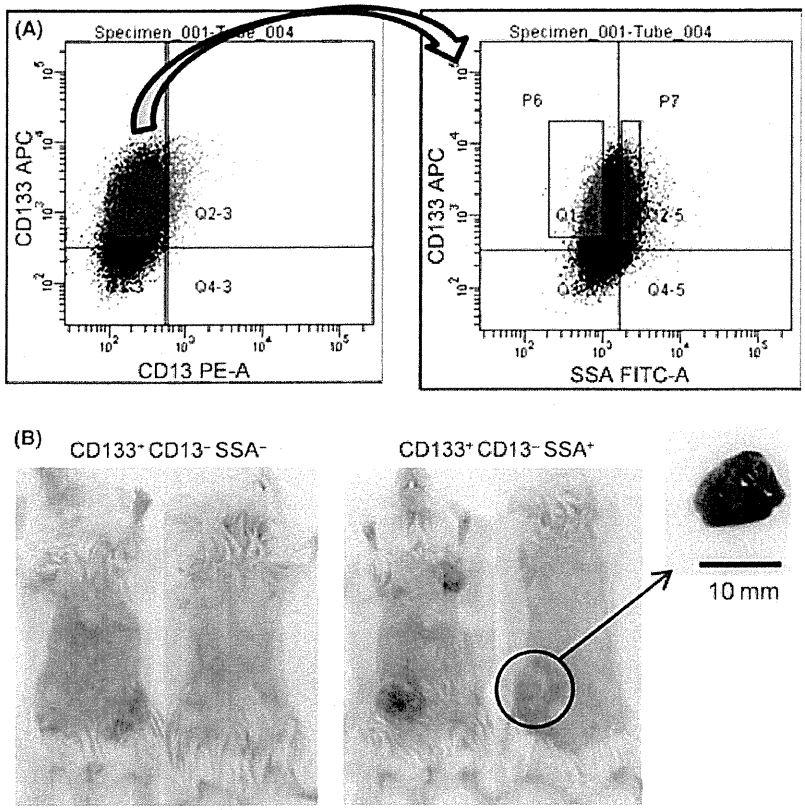

Fig. 5. Tumorigenicity of $CD133^+CD13^-SSA^-$ and $CD133^+CD13^-SSA^+$ cells isolated from Huh7 cells in non-obese diabetic/severe combined immunodeficiency disease (NOD/SCID) mice. (A) $CD133^+CD13^-$ cells were separated into SSA-negative (P6 gate) and SSA-positive (P7 gate) subfractions by FACS sorting. (B) Sorted cells were subcutaneously injected into NOD/SCID mice. A representative example of tumor formation at 30 days after the injection of $CD133^+$ $CD13^-SSA^+$ cells is shown.

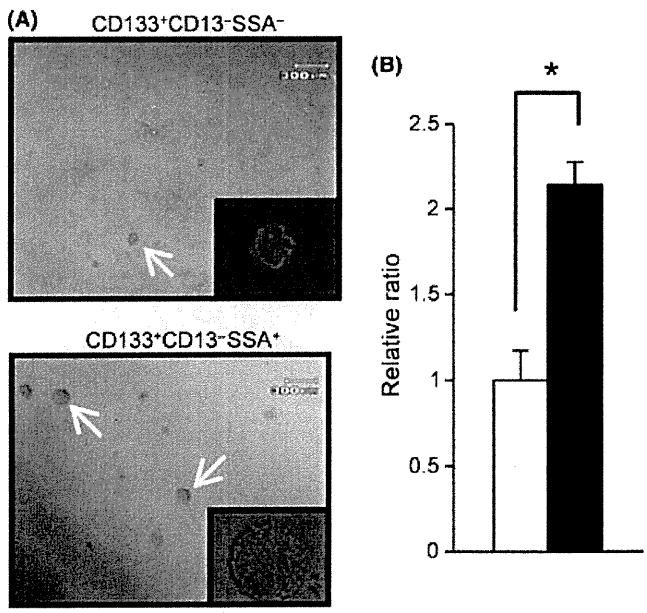

Fig. 6. Spheroid colony formation by $CD133^+CD13^-SSA^-$ and $CD133^+CD13^-SSA^+$ cells. (A) Representative phase-contrast images of spheroids (arrows) derived from individual sorted cells are shown (original magnification, ×40). A representative close-up picture of each spheroid colony is shown in the inset (original magnification, × 400). (B) The ratio of the area of each spheroid colony to the visual field was calculated. $CD133^+CD13^-SSA^-$ and $CD133^+CD13^-SSA^+$ cells are indicated by white and black columns, respectively. Statistical analysis was performed by means of unpaired *t*-test. The asterisk indicates a significant difference ($P < 0.01$).

transcription level analysis. However, it is difficult to detect expressions of most glycogenes by a DNA microarray due to their low expressions. Therefore, in the present study, multiple qPCR array analysis that we previously established was performed to search genes responsible for increased expression of sialylated glycans in $CD133^+CD13^+$ CSC. ST6GALNAC1 stands for α-*N*-acetyl galactosaminide α2,6-sialyltransferase 1 and transfers a sialic acid via an α2,6 linkage to *O*-linked GalNAc residue. The cancer-associated sialyl-Tn (sTn; Neu5Acα2,6GalNAc-*O*-Ser/Thr) antigen is formed by ST6GALNAC1-catalyzed sialylation of GalNAc residues on mucins.[29] Several investigators have reported that expression of the sTn antigen is a poor prognostic factor in patients with adenocarcinoma of the stomach,[30–32] ductal cell carcinoma of the mammary glands[33,34] and epithelial ovarian cancer.[35] Thus, sTn antigen synthesized by ST6GALNAC1 might be associated with the characteristics of CSC.

The lectin microarray showed high affinity of $CD133^+CD13^+$ CSC to both α2,3- and α2,6-sialic acid-recognizing lectins. The increased binding to α2,3-sialic acid-recognizing lectins is not explained by the high expression of ST6GALNAC1. CMP-sialic acid is involved in all types of sialylation as a donor substrate for all sialyltransferases. Because genes of synthetic enzymes of CMP-sialic acid are not carried on the array, these genes and their product, CMP-sialic acid, might be responsible for the increased α2,3-sialylation. In the case of fucosylated glycans, synthesis and transport of GDP-fucose, a donor substrate for all fucosyltransferases, mainly regulates cellular fucosylation in HCC.[36,37]

Several previous studies have shown that sialic acids were associated with normal stem cells. Satomaa *et al.*[38] reported that the surface of human ES cells were clearly labeled by MAA lectin, which recognizes structures containing α2,3-linked sialic

doi: 10.1111/j.1349-7006.2011.01923.x

acids, preferably α2,3-sialylated *N*-acetyllactosamine, indicating that such sialylated glycans were abundant on the surface of human ES cells. In addition, the heavily glycosylated sialomucin molecule CD34 is known to be expressed on virtually all hematopoietic precursor cells, including multipotent stem cells.[39] Moreover, podocalyxin, which is a sialoglycoprotein structurally related to CD34, is highly expressed on embryonic stem cells,[40] and has been suggested to be a cell surface marker for hemangioblasts, the common precursors of hematopoietic and endothelial cells.[41] Because normal stem cells and CSC are considered to share similar self-renewal programs, these data suggest the involvement of sialylated glycans in the stem/progenitor cell property of CSC. It has remained unclear how sialylated glycans regulate CSC's ability. Identification of molecules carrying sialylated glycans in $CD133^+CD13^+$ CSC would facilitate the understanding of the function of sialylated glycans in the characteristics of CSC.

In the present study, we demonstrated that $CD133^+CD13^-SSA^+$ cells from liver cancer cell lines, Huh7 and Hep3B, exhibited high CSC ability compared with $CD133^+CD13^-SSA^-$ cells (Figs 5,6 and Table S2). These results indicate that $CD133^+CD13^-SSA^+$ cells as well as $CD133^+CD13^+$ cells have sufficient ability to give rise to new tumors. These results suggest the existence of CD13-negative CSC among liver cancer. Recently, several studies revealed that $EpCAM^+$,[42] $CD133^+CD44^+$[43] and $BMI1^+$ cells[44] are hepatic tumor-initiating cells with stem/progenitor cell features, and that these molecules can be used as CSC markers to isolate CSC from HCC cell lines.[45] Thus, the $CD133^+CD13^-SSA^+$ population might include these other types of hepatic CSC. Because $CD13^+$ cells were definitely enriched in the SSA-positive population, as shown in Figure 3, the $CD133^+SSA^+$ population includes both $CD133^+CD13^+$ CSC and other types of CSC such as $EpCAM^+$, $CD133^+CD44^+$ and/or $BMI1^+$ cells. Therefore, $CD133^+SSA^+$ cells might be a more suitable and attractive target for the development of more effective therapies for HCC. In addition, this finding indicates that glycan-recognizing lectins are valuable tools for isolating small subsets of cells, such as stem cells. Actually, we previously reported that the isolation of hepatic progenitor cells from liver tissues of rats with fulminant hepatitis was achieved by the use of E_4PHA lectin.[46] Thus, SSA lectin would be a useful tool for isolating CSC from tumor tissues.

Acknowledgments

The present study was supported by the innovation promotion program of the New Energy and Industrial Technology Development Organization and the Global-Center of Excellence (G-COE) Program of Osaka University School of Medicine.

Disclosure Statement

Shunsaku Takeishi is an employee of GP Bioscience Ltd. Other authors have no conflict of interest.

References

1 Reya T, Morrison SJ, Clarke MF, Weissman IL. Stem cells, cancer, and cancer stem cells. *Nature* 2001; **414**: 105–11.
2 Ailles LE, Weissman IL. Cancer stem cells in solid tumors. *Curr Opin Biotechnol* 2007; **18**: 460–6.
3 Clarke MF, Dick JE, Dirks PB *et al.* Cancer stem cells – perspectives on current status and future directions: AACR workshop on cancer stem cells. *Cancer Res* 2006; **66**: 9339–44.
4 Dean M, Fojo T, Bates S. Tumour stem cells and drug resistance. *Nat Rev Cancer* 2005; **5**: 275–84.
5 Bao S, Wu Q, McLendon RE *et al.* Glioma stem cells promote radioresistance by preferential activation of the DNA damage response. *Nature* 2006; **444**: 756–60.
6 Lapidot T, Sirard C, Vormoor J *et al.* A cell initiating human acute myeloid leukaemia after transplantation into SCID mice. *Nature* 1994; **367**: 645–8.
7 Al-Hajj M, Wicha MS, Benito-Hernandez A, Morrison SJ, Clarke MF. Prospective identification of tumorigenic breast cancer cells. *Proc Natl Acad Sci U S A* 2003; **100**: 3983–8.
8 Singh SK, Hawkins C, Clarke ID *et al.* Identification of human brain tumour initiating cells. *Nature* 2004; **432**: 396–401.
9 Galli R, Binda E, Orfanelli U *et al.* Isolation and characterization of tumorigenic, stem-like neural precursors from human glioblastoma. *Cancer Res* 2004; **64**: 7011–21.
10 Patrawala L, Calhoun T, Schneider-Broussard R *et al.* Highly purified CD44+ prostate cancer cells from xenograft human tumors are enriched in tumorigenic and metastatic progenitor cells. *Oncogene* 2006; **25**: 1696–708.
11 O'Brien CA, Pollett A, Gallinger S, Dick JE. A human colon cancer cell capable of initiating tumour growth in immunodeficient mice. *Nature* 2007; **445**: 106–10.
12 Ricci-Vitiani L, Lombardi DG, Pilozzi E *et al.* Identification and expansion of human colon-cancer-initiating cells. *Nature* 2007; **445**: 111–5.
13 Dalerba P, Dylla SJ, Park IK *et al.* Phenotypic characterization of human colorectal cancer stem cells. *Proc Natl Acad Sci U S A* 2007; **104**: 10158–63.
14 Li C, Heidt DG, Dalerba P *et al.* Identification of pancreatic cancer stem cells. *Cancer Res* 2007; **67**: 1030–7.
15 Wu Y, Wu PY. CD133 as a marker for cancer stem cells: progresses and concerns. *Stem Cells Dev* 2009; **18**: 1127–34.
16 Haraguchi N, Ohkuma M, Sakashita H *et al.* CD133+CD44+ population efficiently enriches colon cancer initiating cells. *Ann Surg Oncol* 2008; **15**: 2927–33.
17 Haraguchi N, Ishii H, Mimori K *et al.* CD13 is a therapeutic target in human liver cancer stem cells. *J Clin Invest* 2010; **120**: 3326–39.
18 Fuster MM, Esko JD. The sweet and sour of cancer: glycans as novel therapeutic targets. *Nat Rev Cancer* 2005; **5**: 526–42.
19 Haltiwanger RS, Lowe JB. Role of glycosylation in development. *Annu Rev Biochem* 2004; **73**: 491–537.
20 Solter D, Knowles BB. Monoclonal antibody defining a stage-specific mouse embryonic antigen (SSEA-1). *Proc Natl Acad Sci U S A* 1978; **75**: 5565–9.
21 Muramatsu T, Muramatsu H. Carbohydrate antigens expressed on stem cells and early embryonic cells. *Glycoconj J* 2004; **21**: 41–5.
22 Varki A. Sialic acids in human health and disease. *Trends Mol Med* 2008; **14**: 351–60.
23 Yogeeswaran G, Salk PL. Metastatic potential is positively correlated with cell surface sialylation of cultured murine tumor cell lines. *Science* 1981; **212**: 1514–6.
24 Fogel M, Altevogt P, Schirrmacher V. Metastatic potential severely altered by changes in tumor cell adhesiveness and cell-surface sialylation. *J Exp Med* 1983; **157**: 371–6.
25 Passaniti A, Hart GW. Cell surface sialylation and tumor metastasis. Metastatic potential of B16 melanoma variants correlates with their relative numbers of specific penultimate oligosaccharide structures. *J Biol Chem* 1988; **263**: 7591–603.
26 Kuno A, Uchiyama N, Koseki-Kuno S *et al.* Evanescent-field fluorescence-assisted lectin microarray: a new strategy for glycan profiling. *Nat Methods* 2005; **2**: 851–6.
27 Ito H, Kuno A, Sawaki H *et al.* Strategy for glycoproteomics: identification of glyco-alteration using multiple glycan profiling tools. *J Proteome Res* 2009; **8**: 1358–67.
28 Narimatsu H, Sawaki H, Kuno A, Kaji H, Ito H, Ikehara Y. A strategy for discovery of cancer glyco-biomarkers in serum using newly developed technologies for glycoproteomics. *FEBS J* 2010; **277**: 95–105.
29 Ikehara Y, Kojima N, Kurosawa N *et al.* Cloning and expression of a human gene encoding an *N*-acetylgalactosamine-alpha2,6-sialyltransferase (ST6GalNAc I): a candidate for synthesis of cancer-associated sialyl-Tn antigens. *Glycobiology* 1999; **9**: 1213–24.
30 Ma XC, Terata N, Kodama M, Jancic S, Hosokawa Y, Hattori T. Expression of sialyl-Tn antigen is correlated with survival time of patients with gastric carcinomas. *Eur J Cancer* 1993; **29A**: 1820–3.
31 Werther JL, Rivera-MacMurray S, Bruckner H, Tatematsu M, Itzkowitz SH. Mucin-associated sialosyl-Tn antigen expression in gastric cancer correlates with an adverse outcome. *Br J Cancer* 1994; **69**: 613–6.
32 Werther JL, Tatematsu M, Klein R *et al.* Sialosyl-Tn antigen as a marker of gastric cancer progression: an international study. *Int J Cancer* 1996; **69**: 193–9.
33 Soares R, Marinho A, Schmitt F. Expression of sialyl-Tn in breast cancer. Correlation with prognostic parameters. *Pathol Res Pract* 1996; **192**: 1181–6.
34 Kinney AY, Sahin A, Vernon SW *et al.* The prognostic significance of sialyl-Tn antigen in women treated with breast carcinoma treated with adjuvant chemotherapy. *Cancer* 1997; **80**: 2240–9.

35 Kobayashi H, Terao T, Kawashima Y. Serum sialyl Tn as an independent predictor of poor prognosis in patients with epithelial ovarian cancer. *J Clin Oncol* 1992; **10**: 95–101.
36 Noda K, Miyoshi E, Gu J *et al.* Relationship between elevated FX expression and increased production of GDP-L-fucose, a common donor substrate for fucosylation in human hepatocellular carcinoma and hepatoma cell lines. *Cancer Res* 2003; **63**: 6282–9.
37 Moriwaki K, Noda K, Nakagawa T *et al.* A high expression of GDP-fucose transporter in hepatocellular carcinoma is a key factor for increases in fucosylation. *Glycobiology* 2007; **17**: 1311–20.
38 Satomaa T, Heiskanen A, Mikkola M *et al.* The *N*-glycome of human embryonic stem cells. *BMC Cell Biol* 2009; **10**: 42.
39 Terstappen LW, Huang S, Safford M, Lansdorp PM, Loken MR. Sequential generations of hematopoietic colonies derived from single nonlineage-committed CD34+CD38$^-$ progenitor cells. *Blood* 1991; **77**: 1218–27.
40 Choo AB, Tan HL, Ang SN *et al.* Selection against undifferentiated human embryonic stem cells by a cytotoxic antibody recognizing podocalyxin-like protein-1. *Stem Cells* 2008; **26**: 1454–63.
41 Hara T, Nakano Y, Tanaka M *et al.* Identification of podocalyxin-like protein 1 as a novel cell surface marker for hemangioblasts in the murine aorta-gonad-mesonephros region. *Immunity* 1999; **11**: 567–78.
42 Yamashita T, Ji J, Budhu A *et al.* EpCAM-positive hepatocellular carcinoma cells are tumor-initiating cells with stem/progenitor cell features. *Gastroenterology* 2009; **136**: 1012–24.
43 Zhu Z, Hao X, Yan M *et al.* Cancer stem/progenitor cells are highly enriched in CD133+CD44+ population in hepatocellular carcinoma. *Int J Cancer* 2010; **126**: 2067–78.
44 Chiba T, Miyagi S, Saraya A *et al.* The polycomb gene product BMI1 contributes to the maintenance of tumor-initiating side population cells in hepatocellular carcinoma. *Cancer Res* 2008; **68**: 7742–9.
45 Yi SY, Nan KJ. Tumor-initiating stem cells in liver cancer. *Cancer Biol Ther* 2008; **7**: 325–30.
46 Sasaki N, Moriwaki K, Uozumi N *et al.* High levels of E4-PHA-reactive oligosaccharides: potential as marker for cells with characteristics of hepatic progenitor cells. *Glycoconj J* 2009; **26**: 1213–23.

Supporting Information

Additional Supporting Information may be found in the online version of this article:

Fig. S1. Differential glycan profiling of CD133$^+$CD13$^-$ and CD133$^+$CD13$^+$ cells isolated from Hep3B cells using a lectin microarray.

Fig. S2. Focused differential glycan profiling of CD133$^+$CD13$^-$ and CD133$^+$CD13$^+$ cells isolated from Hep3B cells.

Table S1. Differential expression profiling of 186 glycogenes between CD133$^+$CD13$^-$ and CD133$^+$CD13$^+$ cells.

Table S2. The tumor-initiating ability of CD133$^+$CD13$^-$SSA$^-$ and CD133$^+$CD13$^-$SSA$^+$ cells among Hep3B cells.

Please note: Wiley-Blackwell are not responsible for the content or functionality of any supporting materials supplied by the authors. Any queries (other than missing material) should be directed to the corresponding author for the article.

doi: 10.1111/j.1349-7006.2011.01923.x

Published OnlineFirst January 10, 2011; DOI:10.1158/1078-0432.CCR-10-2132

Clinical Cancer Research

MicroRNA-125a-5p Is an Independent Prognostic Factor in Gastric Cancer and Inhibits the Proliferation of Human Gastric Cancer Cells in Combination with Trastuzumab

Naohiro Nishida, Koshi Mimori, Muller Fabbri, et al.

Clin Cancer Res 2011;17:2725-2733. Published OnlineFirst January 10, 2011.

Published OnlineFirst January 10, 2011; DOI:10.1158/1078-0432.CCR-10-2132

Clinical Cancer Research

MicroRNA-125a-5p Is an Independent Prognostic Factor in Gastric Cancer and Inhibits the Proliferation of Human Gastric Cancer Cells in Combination with Trastuzumab

Naohiro Nishida[1,2], Koshi Mimori[1], Muller Fabbri[3], Takehiko Yokobori[1], Tomoya Sudo[1], Fumiaki Tanaka[1], Kohei Shibata[1], Hideshi Ishii[1,2], Yuichiro Doki[2], and Masaki Mori[1,2]

Abstract

Purpose: MicroRNA 125a-5p (*miR-125a-5p*) has been reported to be a tumor suppressor in malignancies of the breast, ovary, lung, and central nervous system. However, the clinical significance of *miR-125a-5p* in human gastrointestinal cancer has not been explored. We investigated a tumor inhibitory effect of *miR-125a-5p* in gastric cancer, focusing in particular on the *miR-125a-ERBB2* (*HER2, HER-2/neu*) pathway.

Experimental Design: Quantitative RT-PCR was used to evaluate *miR-125a-5p* expression in 87 gastric cancer cases to determine the clinicopathologic significance of *miR-125a-5p* expression. The regulation of *ERBB2* by *miR-125a-5p* was examined with precursor *miR-125a*–transfected cells. Furthermore, we investigated whether *miR-125a-5p* suppresses proliferation of gastric cancer cells in combination with trastuzumab, a monoclonal antibody against ERBB2.

Results: Low expression levels of *miR-125a-5p* were associated with enhanced malignant potential such as tumor size ($P = 0.0068$), tumor invasion ($P = 0.031$), liver metastasis ($P = 0.029$), and poor prognosis ($P = 0.0069$). Multivariate analysis indicated that low *miR-125a-5p* expression was an independent prognostic factor for survival. *In vitro* assays showed that *ERBB2* is a direct target of *miR-125a-5p*, which potently suppressed the proliferation of gastric cancer cells, and, interestingly, the growth inhibitory effect was enhanced in combination with trastuzumab.

Conclusions: *miR-125a-5p* is a meaningful prognostic marker. Furthermore, *miR-125a-5p* mimic alone or in combination with trastuzumab could be a novel therapeutic approach against gastric cancer. *Clin Cancer Res; 17(9); 2725–33. ©2011 AACR.*

Introduction

MicroRNAs (miRNA) constitute a class of small (19–25 nucleotides) noncoding RNAs that function as posttranscriptional gene regulators. miRNAs regulate gene expression by binding to their mRNAs (1). Alterations in miRNA expression are involved in the initiation, progression, and metastasis of human cancer, and it is believed that miRNAs function both as tumor suppressors and oncogenes in cancer development (2, 3).

Authors' Affiliations: [1]Department of Surgery and Molecular Oncology, Medical Institute of Bioregulation, Kyushu University, Beppu, Oita; [2]Department of Gastroenterological Surgery, Osaka University Graduate School of Medicine, Suita City, Osaka, Japan; and [3]Department of Molecular Virology, Immunology and Medical Genetics. The Ohio State University Comprehensive Cancer Center, Columbus, Ohio

Note: Supplementary data for this article are available at Clinical Cancer Research Online (http://clincancerres.aacrjournals.org/).

Corresponding Author: Masaki Mori, Department of Gastroenterological Surgery, Osaka University Graduate School of Medicine, 2-2 Yamada-oka, Suita City, Osaka 565-0871, Japan. Phone: 8166-879-3251; Fax; 8166-879-3259; E-mail: mmori@gesurg.med.osaka-u.ac.jp

doi: 10.1158/1078-0432.CCR-10-2132

Recent studies have shown that the expression of *miR125a-5p* is downregulated in several human cancers such as breast cancer (4–6), ovarian cancer (7), lung cancer (8), and medulloblastoma (9). Li and colleagues reported that a germline mutation in mature miRNA 125a-5p (*miR-125a-5p*) is closely associated with breast cancer tumorigenesis (5). Other reports showed that epidermal growth factor (EGF) receptor signaling suppresses *miR-125a-5p* expression and leads to cancer metastasis in lung cancer (8) and ovarian cancer (10). Furthermore, in squamous cell carcinoma of the oral cavity, the levels of *miR-125a-5p* were significantly downregulated in the saliva of patients (11). These findings strongly suggest that the function of *miR-125a-5p* as a tumor suppressor is not organ specific.

Scott and colleagues revealed that *miR-125a-5p* and its homologue, *miR-125b*, regulate *ERBB2* and *ERBB3* in human breast cancer cells (12). In gastric cancer, ERBB2 overexpression has been increasingly recognized as a frequent molecular abnormality and as an important therapeutic target similar to breast cancer (13, 14). Preclinical and clinical data have revealed significant efficacy of anti-ERBB2 therapies, especially trastuzumab (Herceptin), a monoclonal antibody directed at ERBB2 in gastric cancer (15, 16).

Published OnlineFirst January 10, 2011; DOI:10.1158/1078-0432.CCR-10-2132

Translational Relevance

Quantitative real-time reverse transcriptase PCR analysis of microRNA 125a-5p (*miR-125a-5p*) in 87 cases of gastric cancer revealed that low expression levels of *miR-125a-5p* were associated with enhanced malignant potential such as tumor size, tumor invasion, liver metastasis, and poor prognosis. To evaluate the function of *miR-125a-5p*, we focused on the *miR-125a–ERBB2 (HER2, HER-2/neu)* pathway. In gastric cancer, ERBB2 overexpression has been increasingly recognized as an important therapeutic target similar to that in breast cancer. Our data suggested that *miR-125a-5p* directly targets *ERBB2*. *miR-125a-5p* powerfully suppressed the proliferation of gastric cancer cells and, moreover, the growth inhibitory effect was enhanced in combination with trastuzumab, a monoclonal antibody against ERBB2. *miR-125a-5p* is a meaningful prognostic indicator. Furthermore, *miR-125a-5p* mimic alone or in combination with trastuzumab could be a novel therapeutic approach against gastric cancer.

In this study, we showed that *miR-125a-5p* functions as a crucial tumor suppressor in human gastric cancer. Low *miR-125a-5p* expression was correlated with more aggressive disease and poorer prognosis and was an independent prognostic factor. Of the numerous target genes of *miR-125a-5p*, we focused on *ERBB2* and discovered that *miR-125a-5p* regulates *ERBB2* in human gastric cancer cells. *miR-125a-5p* potently suppressed the proliferation of gastric cancer cells. Moreover, the growth inhibitory effect was enhanced in combination with trastuzumab. This is the first report describing the clinical significance of *miR-125a-5p* and its growth inhibitory effect in human gastric cancer.

Materials and Methods

Clinical cases

Patients and sample collection. Eighty-seven gastric cancer samples were obtained during surgery and used after obtaining informed consent. All patients underwent resection of the primary tumor at Kyushu University Hospital at Beppu and affiliated hospitals between 1992 and 2000. Written informed consent was obtained from all patients. All patients had a clear histologic diagnosis of gastric cancer, based on the clinicopathologic criteria described by the Japanese Gastric Cancer Association (17). All patients were closely followed every 3 months. The follow-up periods ranged from 0.2 months to 12.3 years, with a mean of 2.6 years. Resected cancer tissues were immediately cut and embedded in Tissue-Tek OCT (optimum cutting temperature) medium (Sakura), frozen in liquid nitrogen, and kept at −80°C until RNA and DNA extraction. Frozen tissue specimens were homogenized in guanidium thiocyanate, and total RNA was obtained by ultracentrifugation through a cesium chloride cushion. cDNA was synthesized from 8.0 μg of total RNA as previously described (18). Clinicopathologic factors and clinical stage were classified by the criteria of the Japanese Gastric Cancer Association (17). All sample data, including age, gender, tumor size and depth, lymphatic invasion, lymph node metastasis, vascular invasion, liver metastasis, peritoneal dissemination, distant metastasis, clinical stage, and histologic grade, were obtained from the clinical and pathologic records and are summarized in Table 1.

Evaluation of *miR-125a-5p* expression in clinical samples

For *miR-125a-5p* quantitative real-time reverse transcriptase PCR (RT-PCR), cDNA was synthesized from 10 ng of total RNA using TaqMan MicroRNA hsa-*miR-125a-5p* specific primers (Applied Biosystems) and a TaqMan MicroRNA Reverse Transcription kit (Applied Biosystems). RT-PCR protocols are described in Supplementary Data.

Evaluation of *ERBB2*, *DACH1*, and *PDCD6* mRNA expression in gastric cancer cells

For RNA analysis, each cell line was seeded at 2×10^5 cells per well in a volume of 2 mL in 6-well flat-bottomed microtiter plates. Total RNA from cell lines was isolated using the mirVana miRNA Isolation Kit (Ambion) after 48-hour incubation. Quantitative RT-PCR was carried out to measure *ERBB2*, dachshund homolog 1 (*DACH1*), and programmed cell death 6 (*PDCD6*) mRNA expression with the Universal Probe Library Probe (UPL; Roche Diagnostics). Primer sequences corresponding to UPL and RT-PCR protocols are described in Supplementary Data.

Immunohistochemistry

Immunohistochemical studies of ERBB2 were conducted on formalin-fixed, paraffin-embedded (FFPE) surgical sections obtained from patients with gastric cancer. Tissue sections were deparaffinized, soaked in 0.01 mol/L sodium citrate buffer, and boiled in a microwave oven for 5 minutes at 500 W to retrieve cell antigens. Mouse monoclonal antibody against ERBB2 (Epitomics, Inc.) diluted 1:400 was used as the primary antibody. All tissue sections were immunohistochemically stained with the avidin–biotin-peroxidase method (LSAB+ System HRP; Dako, Inc.) and counterstained with hematoxylin.

Evaluation of ERBB2 immunohistochemical staining

The slides were examined and scored independently by 2 experienced pathologists. Evaluation of the results was done according to the criteria recommended by Hofmann and colleagues and other groups (19, 20), by assigning a score from 0 to 3+. Scores were defined as follows: 0, no reactivity or membranous reactivity in less than 10% of ≥ cells; 1+, faintbarely perceptible membranous reactivity in 10% or more of cells; cells are reactive only in part of their membrane; 2+, weak to moderate complete or basolateral membranous reactivity in ≥ 10% or more of tumor cells; 3+, moderate to strong complete or basolateral

Published OnlineFirst January 10, 2011; DOI:10.1158/1078-0432.CCR-10-2132

Table 1. *miR-125a-5p* expression and clinicopathologic factors

Factors	Low expression group ($n = 55$)		High expression group ($n = 32$)		P
	n	%	*n*	%	
Age (mean ± SD)	63.5 ± 1.60		67.2 ± 2.09	0.16	
Sex					
Male	36	65.5	20	62.5	0.78
Female	19	34.5	12	37.5	
Histologic grade					
Well and moderately	21	38.2	17	53.1	0.18
Poorly and others	34	61.8	15	46.9	
Size					
50 mm > (small)	18	32.7	20	62.5	0.0068[a]
50 mm < (large)	37	67.3	12	37.5	
Depth of tumor invasion[b]					
m, sm, mp	12	21.8	21	14	0.031[a]
ss, se, si	43	78.2	11	18	
Lymph node metastasis					
Absent	15	27.3	13	40.6	0.20
Present	40	72.7	19	59.4	
Lymphatic invasion					
Absent	14	25.5	12	37.5	0.24
Present	41	74.5	20	62.5	
Venous invasion					
Absent	41	74.5	21	65.6	0.38
Present	14	25.5	11	34.4	
Liver metastasis					
Absent	50	90.9	32	91.0	0.029[a]
Present	5	9.1	0	9.0	
Peritoneal dissemination					
Absent	45	81.8	27	84.4	0.76
Present	10	18.2	5	15.6	
Clinical stage					
I–II	22	40	21	65.6	0.020[a]
III–IV	33	60	11	34.4	

[a]$P < 0.05$.

[b]Tumor invasion of mucosa (m), submucosa (sm), muscularis propria (mp), subserosa (ss), penetration of serosa (se), and invasion of adjacent strucures (si).

membranous reactivity in ≥ 10% or more of tumor cells. Specimens with scores of 0 and 1+ were regarded as being negative for ERBB2 expression, whereas scores of 2+ and 3+ indicated positive expression of ERBB2.

Experimental studies

Cell lines and cell culture. The human gastric cancer cell lines AZ521, KATO, MKN1, MKN45, MKN74, NUGC3, and NUGC4 were provided by the Cell Resource Center of Biomedical Research, Institute of Development, Aging and Cancer, Tohoku University. These cell lines were maintained in RPMI 1640 containing 10% FBS with 100 units/mL penicillin and 100 units/mL streptomycin sulfates and cultured in a humidified 5% CO_2 incubator at 37°C.

Transfection of miRNA-125a precursor (*Pre-miR-125a*)

Using NUGC4, a gastric cancer cell line that expresses a high level of *ERBB2* mRNA, either *Pre-miR-125a* or *Pre-miR* negative control (Ambion Pre-miR miRNA Precursors Applied Biosystems), was transfected at 30 nmol/L (final concentration) by using Lipofectamine RNAiMAX (Invitrogen Life Technologies) according to the manufacturer's instruction.

In vitro assays

The MTT assay for gastric cancer cell growth after transfection with *Pre-miR-125a* with/without trastuzumab treatment.

Logarithmically growing NUGC4 cells were transfected with *Pre-miR-125a* or *Pre-miR* negative control with or

Published OnlineFirst January 10, 2011; DOI:10.1158/1078-0432.CCR-10-2132

without addition of trastuzumab (0.1 or 1 μg/mL) and were seeded at 8.0×10^3 cells per well in 96-well flat-bottomed microtiter plates in a final volume of 100 μL of culture medium per well. Cells were incubated in a humidified atmosphere (37°C and 5% CO_2) for 24, 48, 72, and 96 hours after initiation of transfection. MTT assays were used to measure cell proliferation at each period, as described in Supplementary Data. The assay was carried out with 6 replicates.

Plasmid construction

The 3′ untranslated region (3′-UTR) and open reading frame (ORF) of *ERBB2* was amplified by RT-PCR. The amplified product was subcloned and ligated into the pmirGLO Dual-Luciferase miRNA Target Expression Vector (Promega). The resultant reporter vector position was confirmed by sequencing and termed Luc-*ERBB2* WT. To make *miR-125a-5p* binding site mutants, positions 37 to 43 of *ERBB2* 3′-UTR (the sequence; CTCAGGG) were mutated to the sequence CACTGCG (mutated nucleotides are underlined), using the QuikChange Lightning Site-Directed Mutagenesis Kit (Stratagene) according to the manufacturer's protocol. The resultant reporter vector position was confirmed by sequencing and termed Luc-*ERBB2* mutant.

Luciferase assay

Luciferase assays were conducted using 1×10^4 NUGC4 cells plated in a 96-well plate. Transfections were done with Lipofectamine 2000 (Invitrogen) in OptiMEM reduced serum media (GIBCO). Cells were transfected with 30 ng of Luc-*ERBB2* WT vector or Luc-*ERBB2* mutant vector and e100 nmol/L of either *Pre-miR* negative control or *Pre-miR-125a*. Twenty-four hours following transfection, cells were assayed for both firefly and *Renilla* luciferase, using Dual-Glo Luciferase Assay System (Promega). All transfection experiments were conducted in triplicate.

ERBB2 and *miR-125a-5p* expression in the NCI60 panel

For analysis of the correlation between *ERBB2* and *miR-125a-5p* expression in the NCI60 panel (21), the normalized expression levels of the cDNA array and the miRNA array were obtained from the Web site of the Genomics and Bioinformatics Group (http://discover.nci.nih.gov). The data were analyzed by JMP 5 for Windows software (SAS Institute, Inc.).

Protein expression analysis

Western blotting was used to confirm the expression of ERBB2 and phosphorylated AKT, BAK1, and p53 in *Pre-miR-125a*–transfected cells. Primary antibodies and dilutions were as follows: ERBB2 rabbit monoclonal antibody (Epitomics, Inc.) at a 1:500 dilution; AKT rabbit monoclonal antibody (Cell Signaling Technology, Inc.) at a 1:1,000 dilution; phosphorylated AKT (p-AKT) rabbit monoclonal antibody (Cell Signaling Technology, Inc.) at a 1:2,000 dilution; BAK1 (Cell Signaling Technology, Inc.) at a 1:1,000 dilution; p53 (Dako, Inc.) at a 1:1,000 dilution. Detailed protocols are described in Supplementary Data.

Statistical analysis

Data from RT-PCR analysis and *in vitro* transfected cell assays were analyzed with JMP 5. Overall survival rates were calculated actuarially according to the Kaplan–Meier method and were measured from the day of surgery. Differences between groups were estimated using the χ^2 test, Student's *t* test, repeated-measures ANOVA test, and the log-rank test. Variables with a value of $P < 0.05$ in univariate analysis were used in a subsequent multivariate analysis based on the Cox proportional hazards model. A probability level of 0.05 was chosen for statistical significance.

Results

The clinicopathologic significance of *miR-125a-5p* mRNA expression in gastric cancer

In this study, patients with values less than the average expression level of *miR-125a-5p* (8.66, normalized to RNU6B) were assigned to a low expression group ($n = 55$) whereas those with expression values above average were assigned to a high expression group ($n = 32$). Patients in the low *miR-125a-5p* expression group had a significantly poorer prognosis than those in the high *miR-125a-5p* expression group ($P = 0.0069$; Fig. 1). Clinicopathologic factors were significantly different in the low *miR-125a-5p* expression group. There were greater tumor size ($P = 0.0068$), tumor invasion ($P = 0.031$), liver metastasis

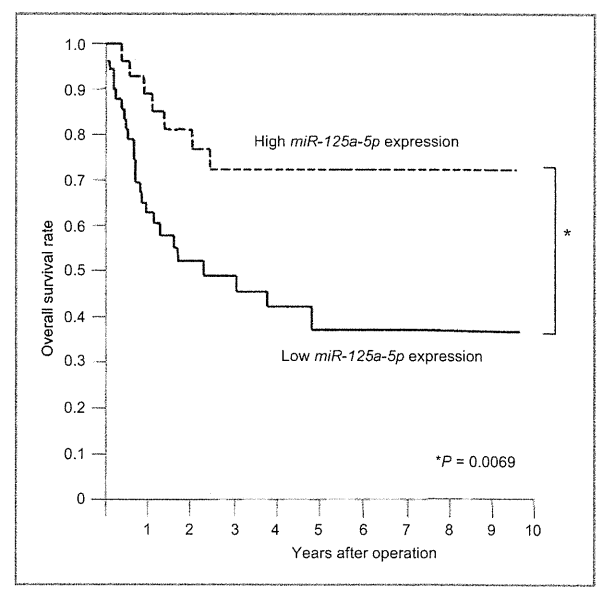

Figure 1. Kaplan–Meier overall survival curves of gastric cancer patients according to the level of *miR-125a-5p* expression. Patients in the low *miR-125a-5p* expression group had a significantly poorer prognosis than those in the high *miR-125a-5p* expression group. The high *miR-125a-5p* expression group ($n = 32$) was composed of patients with higher than average expression levels (8.66, normalized to RNU6B); the low *miR-125a-5p* expression group ($n = 55$) had lower than average expression levels.

Published OnlineFirst January 10, 2011; DOI:10.1158/1078-0432.CCR-10-2132

($P = 0.029$), and clinical staging ($P = 0.02$) than the high *miR-125a-5p* expression group (Table 1). However, no significant differences were observed regarding age, gender, histology, lymphatic invasion, venous invasion, lymph node metastasis, peritoneal dissemination, and distant metastasis (Table 1). The results of univariate and multivariate Cox proportional hazards regression analyses for overall survival are shown in Table 2. Multivariate analysis indicated that the high expression level of *miR-125a-5p* was an independent and significant prognostic factor for survival (OR, 2.44; CI, 1.04–6.73; $P = 0.041$; Table 2). Expression of *ERBB2*, which is a putative *miR-125a-5p* target, is shown to be an indicator of patient prognosis by univariate analysis ($P = 0.048$), although it is not an independent prognostic factor. For the comparison, using the same RNA samples, we also investigated *DACH1 and PDCD6* mRNA expression, which was previously reported as prognostic factors for gastric cancer patients (22). However, in univariate analysis for overall survival, the expression levels of those 2 molecules were not superior to *miR-125a-5p* expression as prognostic factors, at least in the group we investigated (Supplementary Table S1).

ERBB2 mRNA expression in gastric cancer cell lines and the effect of trastuzumab

ERBB2 mRNA expression was examined in 7 gastric cancer cell lines by using RT-PCR. NUGC4, a human cell line derived from a signet ring cell carcinoma of the stomach, showed a remarkably high level of *ERBB2* mRNA compared with other cell lines, ($P < 0.0001$; Supplementary Fig. S1A) and was chosen for experiments on validation of *ERBB2* suppression by *miR-125a-5p*. MTT assays were carried out to evaluate the growth inhibitory effect of trastuzumab in gastric cancer cell lines, NUGC4, AZ521, and NUGC3. AZ521 and NUGC3 were chosen as representative low *ERBB2* expression cell lines. The results indicated that trastuzumab exerted its activity selectively on NUGC4, the *ERBB2* high expression gastric cancer cell line. At the maximum concentration of 100 μg/mL, the cell viability of NUGC4 was reduced by 28.3% ± 3.98% whereas the viability of NUGC3 and AZ521 remained above 90% (Supplementary Fig. S1B).

miR-125a-5p regulates ERBB2 in gastric cancer cells

Using *in silico* miRNA target prediction tools, such as miRanda (23), PicTar (24), and TargetScan (25), we identified the sequence of the *miR-125a-5p* binding sites in the 3′-UTRs of transcripts encoding *ERBB2* (Fig. 2A). To investigate binding and repression, a luciferase reporter assay was carried out with a vector which included the ORF sequence and 3′-UTR of *ERBB2* downstream from the luciferase reporter gene (Luc-*ERBB2* WT). Transient cotransfection of NUGC4 cells with the reporter plasmid and *Pre-miR-125a* significantly reduced luciferase activity in comparison with the negative control ($P < 0.05$). However, the activity of the reporter construct with mutant sequence (Luc-*ERBB2* mutant) was unaffected by simultaneous transfection with *Pre-miR-125a* (Fig. 2B). These data suggest that *ERBB2* mRNA is a direct functional target of *miR-125a-5p*.

miR-125a-5p expression and ERBB2 protein expression in clinical samples

Of the 87 gastric cancer patients we examined for the expression of *miR-125a-5p*, FFPE surgical sections were available in 52 cases. To explore the association between *miR-125a-5p* expression and ERBB2 protein expression status, we carried out immunohistochemical analysis with these samples. The results showed that in the low ERBB2 expression group (ERBB2 staining 0 or 1+; $n = 45$), the expression of *miR-125a-5p* was significantly increased compared with that in the high ERBB2 expression group (ERBB2 staining 2+ or 3+; $n = 7$; mean ± SEM; 4.97 ± 0.88 vs. 2.34

Table 2. Univariate and multivariate analysis for overall survival (Cox proportional regression model)

Factors	Univariate analysis			Multivariate analysis		
	RR	95% CI	*P*	RR	95% CI	*P*
Age (≤65/>66)	0.928	0.648–1.314	0.673	–	–	–
Sex (male/female)	0.834	0.552–1.121	0.345	–	–	–
Histology grade (well, moderately/poorly and others)	1.309	0.913–1.946	0.146	–	–	–
Depth of tumor invasion[a] (m, sm, mp/ss, se, si)	8.387	2.531–51.86	0.0001[b]	2.415	0.650–15.87	0.208
Lymph node metastasis (negative/positive)	4.675	2.162–19.74	0.0001[b]	2.892	1.219–12.88	0.011[b]
Lymphatic invasion (negative/positive)	2.684	1.474–6.676	0.0003[b]	1.177	0.481–5.237	0.761
Venous invasion (negative/positive)	3.324	1.627–6.080	0.0012[b]	1.316	0.883–1.971	0.176
ERBB2 mRNA expression (low/high)	1.466	1.003–2.263	0.0482[b]	1.010	0.991–1.025	0.277
miR-125a-5p expression (high/low)	3.018	1.372–7.588	0.0051[b]	2.438	1.035–6.727	0.041[b]

Abbreviation: RR, Relative risk.

[a]Tumor invasion of mucosa (m), submucosa (sm), muscularis propria (mp), subserosa (ss), penetration of serosa (se), and invasion of adjacent strucures (si).

[b]$P < 0.05$.

Published OnlineFirst January 10, 2011; DOI:10.1158/1078-0432.CCR-10-2132

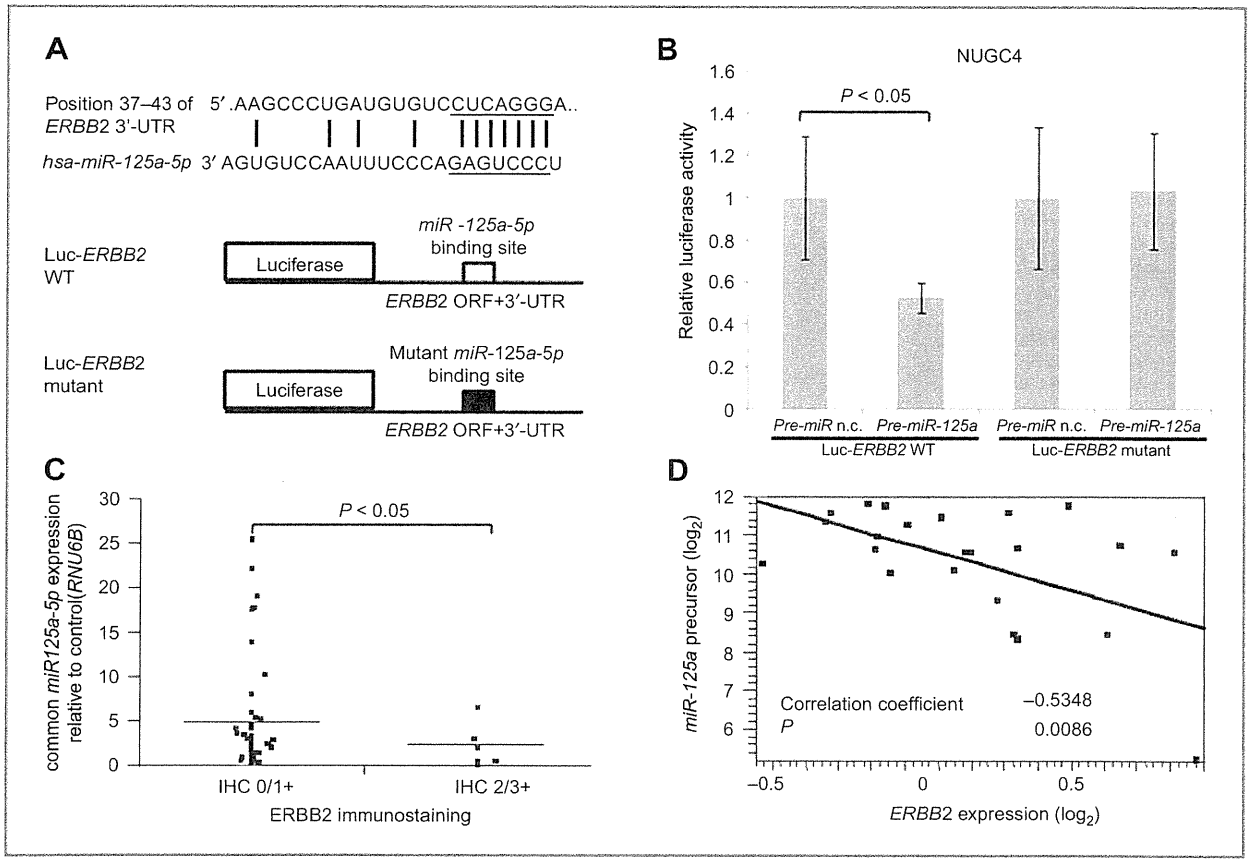

Figure 2. *miR-125a-5p* targets *ERBB2* A, top, sequence of the *miR-125a-5p* binding sites in the 3′-UTRs of transcripts encoding *ERBB2*. Bottom, schematic diagram of the luciferase reporters in target validation. B, *miR-125a-5p* represses its target in the luciferase assay in NUGC4. Relative luciferase level = (Sample Luc/Sample *Renilla*)/(Control Luc/Control *Renilla*). Luc, raw firefly luciferase activity; *Renilla*, internal transfection control *Renilla* activity; *Pre-miR* n.c., *Pre-miR* negative control. The error bar represents the SD from 6 replicates. C, association of *miR-125a-5p* expression with ERBB2 protein expression status determined by immunohistochemical analysis in 52 gastric cancer cases. In the low ERBB2 expression group (ERBB2 staining 0 or 1+; $n = 45$), the expression of *miR-125a-5p* was significantly increased compared with that in the high ERBB2 expression group (ERBB2 staining 2+ or 3+; $n = 7$; P ☒ 0.05). Dots represent the *miR-125a -5p* expression of each sample. Horizontal lines indicate mean value of each group. D, *miR-125a-5p* and *ERBB2* expression levels of carcinoma cells of different origin from the NCI60 tumor cell panel. *ERBB2* expression is inversely correlated with expression of *miR-125a-5p* in 23 cell lines including colon, lung, prostate, and renal cancer.

± 2.24; $P < 0.05$; Fig. 2C). Images of immunohistochemistry are shown in Supplementary Figure S2.

miR-125a-5p and *ERBB2* expression levels in carcinoma cells of different origin from the NCI60 tumor cell panel

To evaluate whether the *miR-125a–ERBB2* pathway functions in cells of different origin, we exploited the cDNA array and the miRNA array data set of NCI60, as described in Material and Methods. *ERBB2* expression was inversely correlated with the expression of *miR-125a-5p* in 23 cell lines including colon, lung, prostate, and renal cancer ($r = -0.5348$, $P = 0.0086$; Fig. 2D).

Both ERBB2 and its primary downstream signal through AKT were suppressed by *miR-125a-5p*

Using RT-PCR, we confirmed that *miR-125a-5p* expression in *Pre-miR-125a*–treated cells was significantly higher than that in untreated cells (parent) and in *Pre-miR negative control*–treated cells ($P < 0.05$, Fig. 3A).To determine whether *miR-125a-5p* suppresses *ERBB2* and its downstream signaling in the gastric cancer cell line NUGC4, cell lysates of transfected cells were analyzed by Western blotting. Remarkable suppression of ERBB2 and phosphorylated AKT (p-AKT) was observed in *Pre-miR-125a*–treated cells, in comparison with untreated cells (parent) or Pre-miR negative control–treated cells (Fig. 3B). However, AKT itself did not show significant reduction. We also investigated the inhibition of previously reported *miR-125a-5p* targets, including apoptosis-related gene *BAK1* (26) and tumor suppressor gene *p53* (27). Western blot analysis showed that protein expression of BAK1 and p53 was moderately suppressed in *Pre-miR-125a*–treated cells; however, the reduction was not as significant as that of ERBB2 (Supplementary Fig. S3).

Published OnlineFirst January 10, 2011; DOI:10.1158/1078-0432.CCR-10-2132

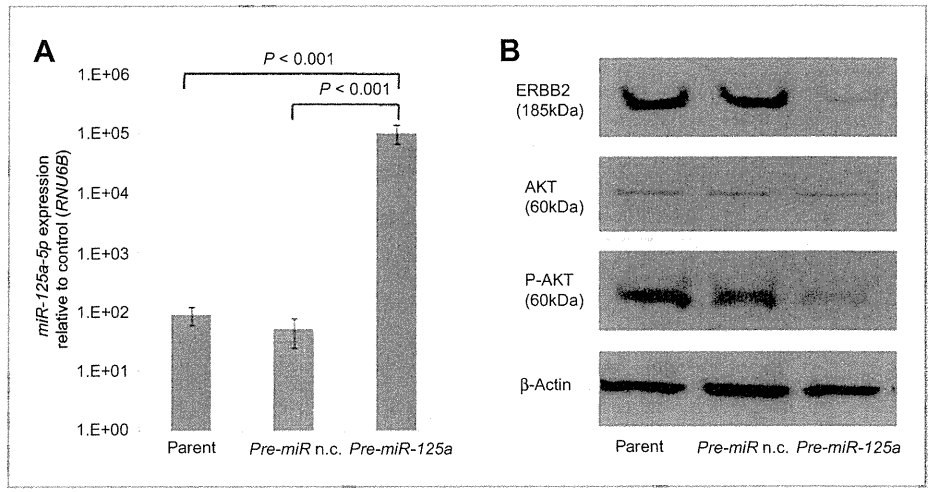

Figure 3. *miR-125a-5p* regulates ERBB2. A, *miR-125a-5p* expression after treatment with negative control or *Pre-miR-125a* in NUGC4 (quantitative RT-PCR). *miR-125a-5p* expression in *Pre-miR-125a*–treated cells is significantly higher than in untreated cells (parent) and in *Pre-miR* negative control–treated cells. The results are the mean ± SD of triplicates. B, Western blotting analysis of ERBB2 and phosphorylated AKT (p-AKT) in NUGC4 cells transfected with *Pre-miR-125a* or negative control (n.c.). These proteins were normalized to the level of β-actin.

miR-125a-5p inhibited the proliferation of gastric cancer cells in combination with trastuzumab

To explain the antitumor efficacy of *miR-125a-5p* in gastric cancer cells, a proliferation assay was carried out with *Pre-miR-125a*–treated cells or negative control cells by using NUGC4. Furthermore, we investigated whether the additional administration of trastuzumab, the ERBB2-targeting antibody, enhanced the antitumor efficacy of *miR-125a-5p*. These experiments were carried out at 2 different concentrations of trastuzumab [0.1 μg/mL (Fig. 4A) and 1 μg/mL (Fig. 4B)]. Interestingly, *miR-125a* not only potently suppressed the proliferation of gastric cancer cells by itself but also inhibited growth more potently when combined with trastuzumab ($P = 0.0032$, Fig. 4A; $P = 0.0033$, Fig. 4B). The combined growth inhibitory effect was more robust at the higher concentration of trastuzumab.

Discussion

Recent evidence has shown that altered patterns of miRNA expression correlate with various human cancers. The behavior of miRNAs is complex because they regulate hundreds of targets, resulting in the downregulation of numerous target genes including oncogenes and tumor suppressors. Therefore, exploring their clinical potential is especially worthwhile.

In the current study, we show that altered *miR-125a-5p* expression significantly affected cancer progression and prognosis in human gastric cancer. Multivariate analysis revealed that *miR-125a-5p* is an independent prognostic factor for survival. Clinicopathologic analysis revealed that low *miR-125a-5p* expression contributes to more advanced tumor size and tumor invasion (Table 1). It

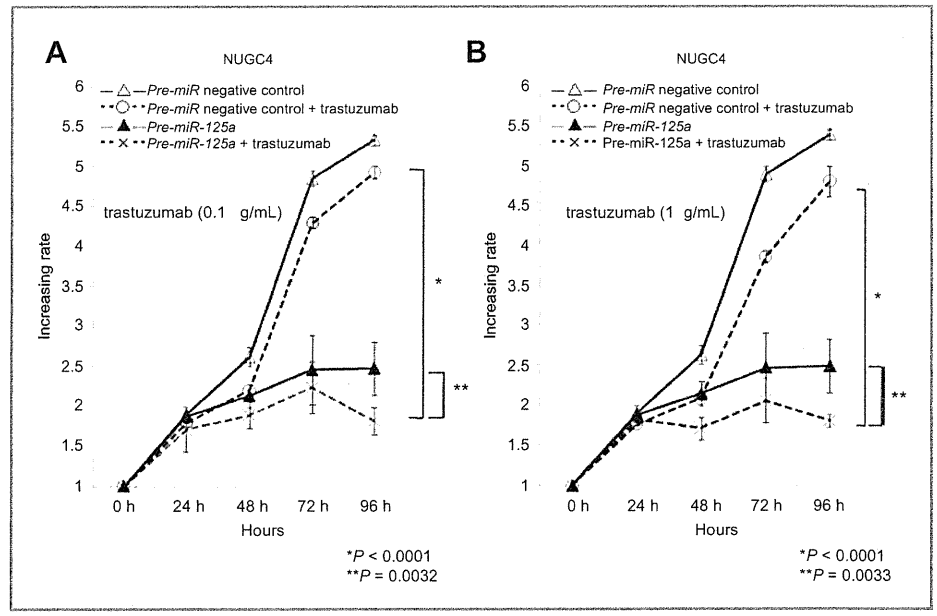

Figure 4. *miR-125a-5p* inhibits the proliferation of the gastric cancer cell line NUGC4 in combination with trastuzumab. *Pre-miR-125a* or *Pre-miR* negative control transfected with or without trastuzumab (A, 0.1 μg/mL; B, 1 μg/mL) treatment were seeded at 8.0×10^3 cells per well in 96-well plates and cell growth was monitored every 24 hours using the MTT assay. Absorbance at 0 hour was assigned a value of 1. The results are the mean ± SD of 3 replicates.